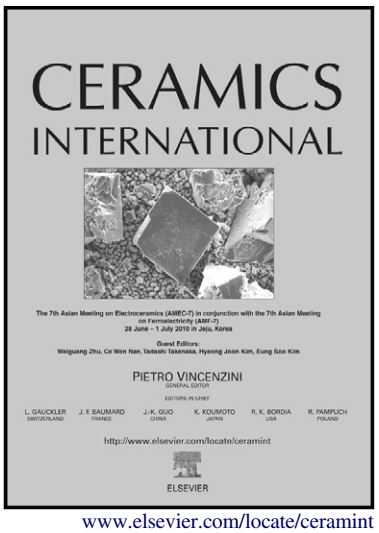

Microwave assisted synthesis of monodispersed Y_2O_3 and Y_2O_3:Eu^{3+} particles

Adrine Malek Khachatourian, Farhad Golestani-Fard, Hossein Sarpoolaky, Carmen Vogt, Muhammet S. Toprak

PII: S0272-8842(14)01490-4
DOI: http://dx.doi.org/10.1016/j.ceramint.2014.09.105
Reference: CERI9224

To appear in: *Ceramics International*

Received date: 14 August 2014
Revised date: 18 September 2014
Accepted date: 19 September 2014

Cite this article as: Adrine Malek Khachatourian, Farhad Golestani-Fard, Hossein Sarpoolaky, Carmen Vogt, Muhammet S. Toprak, Microwave assisted synthesis of monodispersed Y_2O_3 and Y_2O_3:Eu^{3+} particles, *Ceramics International,* http://dx.doi.org/10.1016/j.ceramint.2014.09.105

Microwave assisted synthesis of monodispersed Y_2O_3 and Y_2O_3:Eu^{3+} particles

Adrine Malek Khachatourian[a,b], Farhad Golestani-Fard[b], Hossein Sarpoolaky[b], Carmen Vogt[a,c], Muhammet S. Toprak[a].

[a] Department of Materials and Nano Physics, KTH – Royal Institute of Technology, Kista, Stockholm 16440, Sweden.

[b] School of Metallurgy and Materials Engineering, IUST – Iran University of Science and Technology, Tehran 16846, Iran.

[c] Department of Biomedical and X-ray Physics, KTH – Royal Institute of Technology, Stockholm 10044, Sweden.

Abstract

Monodisperse spherical Y_2O_3 and Y_2O_3:Eu^{3+} nanocrystalline particles with particle size between 100 nm and 350 nm were successfully prepared by microwave assisted urea precipitation method followed by a thermochemical treatment. Fast microwave heating, controlled decomposition of urea and burst nucleation of metal ions in aqueous solution led to the formation of non-aggregated spherical particles with narrow size dispersion. The particle size and size dispersion was controlled by adjusting the urea / metal ions ratio, the metal ions concentration, the reaction time and the temperature. X-ray diffraction (XRD) analysis indicated that the as prepared particles have $Y(OH)CO_3$ composition, which converted to highly crystalline cubic Y_2O_3 after calcination at temperatures above 600°C. The calcined Y_2O_3 particles preserved the spherical morphology of the as prepared particles and exhibited polycrystalline structure. The size of the crystallites increased from ~8 nm to ~37 nm with the increase of the calcination temperature from 500°C to 900°C. In order to transform these nanostructures to luminescent composition, Eu^{3+} doping has been performed. Y_2O_3:Eu^{3+} particles inherited the morphology and polycrystalline structure of the host Y_2O_3 particles. Photoluminescence (PL) analysis of Y_2O_3:Eu^{3+} particles showed a strong red emission peak at 613 nm corresponding to $^5D_0$–$^7F_2$ forced electric dipole transition of Eu^{3+} ions under UV excitation. All these critical characteristics, and being heavy-metal free, make these particles useful for bioimaging, and display devices.

Keywords: A. Microwave processing; Powders: chemical preparation; Calcination; B. Electron microscopy; C. Optical properties; D. Y_2O_3.

1. Introduction

Yttrium oxide (Y_2O_3) is one of the most important advanced ceramic materials that has been investigated for many application areas such as ceramics, optics, magnets, catalysts, superconductors, insulators, and sensors [1]. In addition, Y_2O_3 is a promising host matrix for various triply ionized lanthanide ions (Ln^{3+}) for phosphor industry. Phosphors are made of an inert and chemically stable host doped with small amount of rare earth ions (Re^{3+}) known as optically excited activators [2]. Y_2O_3 is preferred as host material due to its excellent chemical durability, high thermal stability, high refractory property, corrosion resistivity, photochemical stability, broad transparency range (0.2 to 8 μm) with a wide band gap (5.8 eV), high thermal conductivity, low phonon energy, high refractive index and dielectric constant [3,4]. Additionally, similar chemical properties and ionic radius of Y^{3+} and Re^{3+} make it a preferred choice as a host material [5].

Recently, much attention has been paid to the fabrication of Y_2O_3:(Re^{3+}) compounds due to their potential applications in display devices such as cathode ray tubes (CRTs), liquid crystal displays (LCDs), field emission displays (FEDs), and plasma display panels (PDPs) [3,6], temperature sensing devices [7], solid state lasers [8]. Also recently these materials found applications in biomedical area as bio labels [9], bioimaging probes [10], and in medical diagnostics [11]. All these applications demand certain characteristics as single phase with spherical shape and uniform particle size and morphology [5]. For instance, it has been shown that for fluorescence bioimaging the desirable size of the rare earth doped nanophosphors, which are heavy-metal free, should be less than a few hundred nanometers and the size distribution should be narrow [12]. For display applications the smaller the phosphors particle size, the higher the screen resolution [13], and uniform size helps to form a uniform thickness of a phosphor layer on the screen [14]. Critical morphological characteristics of phosphor particles includes nonagglomeration, narrow size distribution and a monodisperse spherical shape [15]. The spherical morphology results in high packing density and reduction of light scattering [16]. However, the reproducible, controlled synthesis of monodisperse spherical Y_2O_3 and Y_2O_3:Re^{3+} particles is still a challenge.

A wide range of synthesis techniques have been developed for the preparation of pure and doped nanocrystalline Y_2O_3 phosphors with different morphologies, including precipitation method [17], sol gel route [18], combustion synthesis [19], hydrothermal process [20], spray pyrolysis method [21], microemulsion method [22], chemical vapor deposition (CVD) technique [23], and microwave assisted synthesis methods [24–27]. Among them, microwave assisted heating systems distinguished as quick, reproducible, simple, and energy efficient method with very short reaction times and higher yield of products. Microwave (MW) irradiation is an emerging efficient heating method where the bulk of the reaction media is heated uniformly, avoiding temperature gradients common in conventional heating. In the microwave assisted heating the energy interacts at molecular levels resulting in a rapid and uniform heating of the reaction mixtures. Comparatively, in the conventional heating systems the heat is generated from external heating sources and transferred through conduction mechanism to the materials surfaces [28–30]. Microwave assisted solution based method has been used for low temperature synthesis of shape-controlled nanocrystals with narrow size distribution.

In this paper we report a microwave assisted urea precipitation method for synthesizing monodisperse nanocrystalline spherical Y_2O_3 and Y_2O_3:Eu^{3+} particles. Metal nitrate powders and urea have been used as inexpensive precursors, without the use of surfactants. To the best of our knowledge there are only few reports on the synthesis of Y_2O_3 submicrometric spherical particles with the microwave method [31,32] but the thorough understanding of the parameters that influences the process has not yet been reported in the literature. We investigated comprehensively the influence of different reaction parameters such as metal ion and urea concentration, reaction temperature and time, and type of mixing. Excellent control of different parameters resulted in well-dispersed monodispersed nanoparticles even after calcination at higher temperatures. Furthermore, we investigated the optimal condition to tailor the particle size and to optimize the crystal structure by controlling the synthetic conditions and further calcination. Finally using the optimized system for Y_2O_3, Y_2O_3:Eu^{3+} particles have been synthesized as a red emitting phosphor.

2. Experimental

2.1 Materials and Methods

Yttrium nitrate hexahydrate, $Y(NO_3)_3.6H_2O$ (Sigma-Aldrich 99.98%), europium nitrate pentahydrate, $Eu(NO_3)_3.5H_2O$ (Sigma-Aldrich 99.99%) and urea (Merck ≥99%) were used as received, without further purification.

Microwave assisted urea precipitation technique was employed to synthesize spherical Y_2O_3 and $Y_2O_3:Eu^{3+}$ nanocrystalline particles. Typically, $Y(NO_3)_3.6H_2O$, $Eu(NO_3)_3.5H_2O$, and urea were dissolved separately in deionized water at room temperature to prepare transparent stock solution of $Y(NO_3)_3$, $Eu(NO_3)_3$ and urea respectively. Then, appropriate amount of each solution have been mixed together. To control the size and monodispersity of Y_2O_3 particles, the concentration of $[Y^{3+}]$ ions in solution varied between 0.02 M to 0.005 M, whereas the molar ratio of urea to $[Y^{3+}]$ ions varied from 5 to 80. The solutions were heated in a Biotage® initiator classic laboratory microwave (Biotage, Uppsala, Sweden), furnace radiation frequency: 2.45 GHz, under magnetic stirring for 5 to 60 minutes at different temperatures (80°C-100°C). The resulting precipitates were separated by centrifugation (8000 rpm), washed with dionized water (Millipore, 15 MΩcm) and ethanol (99,5%, Solveco) twice, then dried at 60°C overnight. After drying, the fine white powders were calcined in air at various temperatures ranging from 300°C to 900°C for 2 hours. In case of $Y_2O_3:Eu^{3+}$ particles the concentration of metal ions (Y^{3+}+Eu^{3+}), molar ratio of urea to metal ions and molar ratio of $[Y^{3+}]$ to $[E^{3+}]$ were fixed at 0.05 M, 50, and 20 respectively and calcination temperature was 900°C.

2.2 Characterizations

The size and morphology of precursors and calcined powders were characterized by JEOL JEM-2100F field emission transmission electron microscopy (TEM) operating at an accelerating voltage of 200 kV (JEOL Ltd., Tokyo, Japan). The powders were dispersed in ethanol, sonicated for 1 minute and dropped onto a carbon coated TEM grid allowing to dry at room temperature. The mean size diameter and standard deviation (SD) were calculated after measuring at least 300 particles in random fields of view on the TEM micrographs.

The phase identification was performed using Powder X-ray diffraction (XRD) on a PAN analytical X'Pert Pro powder diffractometer with Cu-Kα radiation (45 kV, 35 mA). Fourier Transform Infrared Spectroscopy (FTIR) analysis of samples was recorded using Nicolet iS10 spectrophotometer (Thermo scientific, USA) and scans were performed in the range of 525–4000 cm^{-1}. Thermogravimetric analysis (TGA) was carried out using TGA-Q500 (TA instruments, USA), in air atmosphere in the temperature range of 20-1000°C with a heating rate of 10 °C/min. Optical absorption of samples were measured using Perkin Elmer Lambda 750 UV–Vis spectrometer (Perkin Elmer, Shelton, USA). The samples were dispersed in water and pure deionized water was used as reference and the spectra were recorded from 200 nm to 700 nm. The Photoluminescence spectra (PL), was recorded using Perkin–Elmer LS 55 fluorescence spectrometer (Perkin Elmer, Shelton, USA). Samples were dispersed in deionized water and the spectra were recorded from 550 nm to 680 nm.

3. Results and discussion

The optimisation of different reaction parameters and their effect on the particle characteristics was investigated. Moreover the morphological and structural characterisation of the prepared particles was studied and as a proof of concept, Eu doped Y_2O_3 partices were synthesised and characterised.

3.1 Effect of reaction parameters on as prepared particles size, size distribution and morphology

3.1.1. Effect of urea concentration

The effect of urea concentration in the synthesis of the as prepared particles was investigated. The molar ratio of [urea]/[Y^{3+}], designated hereafter ***u***, was varied from 10 to 80, maintaining the [Y^{3+}] concentration (0.005 M), and the reaction time (15 minutes) constant while the reaction temperature was varied from 80°C to 100°C. At ***u*** 10 (Fig. 1a) synthesized nanoparticles have a wide size distribution with a SD up to 100 nm. The polydispersity is maintained even if the temperature is increased or decreased, probably due to low amount of urea for a monodisperse system (Fig. S1). However, increasing the ***u*** above 10 in the solution resulted in homogeneous and monodisperse spherical particles without any agglomeration (Fig. 1c-1f). This same trend of polydispersity at lower ***u*** and monodispersity at higher ***u*** has

been observed when the [Y^{3+}] concentration was 0.01 M and 0.02 M with 15 minutes reaction time (Fig. S2 and S3, respectively).

In conventional urea precipitation method the reaction mechanism comprises three distinct steps: decomposition of urea, hydrolysis of yttrium ions and precipitation of hydroxycarbonate precursor. The formation of solid phase is governed by controlled generation of precipitating ligands mainly OH^- and CO_3^{2-} ions thorough the slow and homogeneous decomposition of urea at temperatures above 80°C [14,33]. For the particles synthesis, all reactant solutions heated up to the desired reaction temperature in less than 90 seconds using fast and homogenous microwave heating. This generates heat by rapid kinetics of the dipole moments of the molecules leading to voluminous heating within few minutes of the reaction. The heating profile of one of the samples is shown in Fig. S4. The monodispersity of particles synthesized by microwave method with the optimised ratio of ***u*** (above 10) can be explained by the fact that the fast heating caused rapid decomposition of large amount of urea followed by quick increase in solution pH. The burst nucleation resulted in particles with uniform size and spherical shape.

A summary of the mean particle size of monodisperse particles synthesized at different reaction conditions is presented in Table 1. Particle size as a function of temperature for different ***u*** is shown in Fig. 2a and 2b for particles with [Y^{3+}] concentration of 0.005M and 0.02M, respectively.

Experimentally, a relation between ***u*** and the final particle size was observed. By increasing the ***u*** the size of the particles decreases for a fixed [Y^{3+}] concentration. This can be explained by a higher degree of supersaturation, which implies a burst formation of nuclei, due to the presence of more OH^- and CO^{2-} in high concentration. Thus at the fixed [Y^{3+}] concentration a high concentration of nucleus led to a decrease in final particle size. This is in accordance with previous observations that a controlled number of nucleus in the initial precipitation stage by optimising urea concentration resulted in the posibility of adjusting the sizes of particles formed [34]. Further increase of urea concentration above an optimum concentration will result in obtaining bigger particles.

3.1.2. Effect of reaction temperature

Further, the effect of the reaction temperature on the size and polydispersity of the obtained nanoparticles was investigated. The reaction temperature influences dramaticaly the urea decomposition and experimentaly we found that the optimum temperature is 90°C that resulted in small monodispersed particles. At higher and lower ***u*** changing the reaction temperature from 90°C to 80°C or 90°C to 100°C resulted in an increase of particle size. We propose that at 80°C urea is not fully decomposed and consequently the burst nucleation is not efficient and bigger particles are obtained. Especially at lower ***u*** in which at 90°C, the complete decomposition of urea led to monodisperse particles (Fig. 1c, S2c, S3c), decreasing the temperature to 80°C resulted in polydisperse particles (Fig. 1b, S2b, S3b). Comparatively, higher temperature (100°C) will accelerate the particles growth rate. Moreover, although the system was sealed, at 100°C CO_2 and H_2O in the form of gasses were generated resulting in a decrease in the liquid phase of the initial concentration of OH^- and CO_3^{2-} ions which are critical for hydrolysis and precipitation reactions. At this temperature, for a fixed $[Y^{3+}]$ concentration, the density of the formed nuclei was lower and bigger particles were produced. Furthermore, at higher ***u*** the morphology of the particles synthesized at 100°C changed from spherical to rough/coarse probably due to higher temperature and higher pH produced from larger amount of urea decomposition (Fig. 1f).

3.1.3. Effect of $[Y^{3+}]$ concentration

The effect of $[Y^{3+}]$ concentration in the reaction solution was investigated. It was observed that for a fixed urea concentration (for example 0.04 M) as the $[Y^{3+}]$ concentration increased (from 0.005 M to 0.02 M) the average sizes of the obtained particles increased also (from 225±24 nm to 323±34 nm) (Fig. 3a). This can be explained by the fact that for a fixed urea concentration the number of nuclei is fixed and an increase in number of cations will result in an increase of the size of the particles/nuclei [33,35].

3.1.4. Effect of time

A relation between the reaction time and the obtained particles size was experimentaly observed. In the case of microwave synthesized particles, after short reaction times (5 min) a stable particle suspension is formed compared to the conventional precipitation method where usually several hours of reaction time is needed. By increasing the reaction time from 5 min to 30 min the particles size increased from 224±24 nm to 258±27 nm for fixed $[Y^{3+}]$ concentration (0.01 M) and ***u*****=**40 (Fig. 3b). During the reaction the number of nuclei was

constant and the spherical crystals become bigger due to continued growth. Additionaly, longer reaction times (above 45 min) resulted in a change in the surface morphology of particles from smooth to rough, probably due to high pH that causes dissolution and precipitation (Fig. S5a,S5b). Consequently, the optimum synthesis time for obtaining particles with spherical morphology is in the range of 5 min to 30 min.

3.1.5. Effect of mixing

The effect of mixing during the reaction was also investigated. The mixing rate used during the typical reactions were 600 rpm. Changing the mixing speed from 600 rpm to 900 rpm did not affect the shape and size of the particles. However a turbulent mixing affected the surface morphology and/or the size monodispersity resulting in particles with a rough surface and a wider size distribution (Fig. S5c) probably due to local concentration variation during the growth phase of the nanoparticles.

3.2 Structural analysis of as prepared and calcined particles

3.2.1. *Thermogravimetric analysis*

TGA was used for analysing the stability of as prepared particles. Thermal decomposition behaviour of particles obtained with two different ***u*** of 5 and 20 is very similar, both types of particles having a total weight loss around 34% indicating that ***u*** has no effect on the composition of the particles (Fig. 4). The particles exhibit a continous weight loss from 100°C to 850°C. Above 850°C the residual weight loss remained constant which means that the hydroxycarbonate form has totally decomposed and converted to the oxide form.

Sordelet et al [33] suggested that the hydroxycarbonate precipitate obtained by conventional urea precipitation method underwent two-step decomposition and converted to oxide as shown by the reactions given below:

$$2Y(OH)CO_{3\,(s)} \rightarrow Y_2O_2CO_{3(s)} + H_2O_{\,(g)} + CO_{2\,(g)}$$

$$Y_2O_2CO_{3(s)} \rightarrow Y_2O_{3(s)} + CO_{2\,(g)}$$

The combined theoretical weight loss for the above reactions is about 32%, which is in agreement with the experimental weight loss considering about 2% weight loss due to the loss of adsorbed water [33,35].

3.2.2. Fourier Transform Infrared Spectroscopy (FTIR)

As prepared air dried nanoparticles and the calcined particles at different temperatures (from 300°C to 900°C) were analysed by FTIR (Fig. 5). In the IR spectra of the as prepared particles and the particles calcined at 300°C the absorption bands at about 3523 cm^{-1} and 3495 cm^{-1} are assigned to the stretching vibration of OH^- group (OH υ), the bonds around 1520 cm^{-1} and 1430 cm^{-1} result from C-O asymmetric stretching vibration (CO υ_{as}) in CO_3^{2-} and the symmetric stretch of C-O in CO_3^{2-} (CO υ_{as}) is around 1085 cm^{-1}, while the absorptions peaks at 850, 836 cm^{-1} and 728, 712 cm^{-1} are assigned to deformation vibration of C-O (CO δ) and their splitting [36,37]. There are no absorption bands observed for HCO_3^- and NO_3^- groups in the spectra suggesting the composition of the as prepared particles are $Y(OH)CO_3$ and they maintain the same structure till 300°C [9]. After calcining at 500°C the peaks corresponding to C-O and O-H vibrations reduce in intensity and disappear completely at 800°C – 900°C. From 600°C a new sharp peak appears at 560 cm^{-1} which is assigned to Y-O stretching vibration and the formation of Y_2O_3 [4]. Increasing the calcination temperature the absorption peak at 560 cm^{-1} becomes stronger and at 800°C the hydroxycarbonate precursors decomposed totally, converting to the oxide form.

3.2.3. Powder X-ray diffraction (XRD)

Further, the phase of the as prepared and calcined particles was identified by XRD (Fig. 6). As prepared powders have all diffraction peaks indexed to orthorhombic phase of $Y(OH)CO_3$ (JCPDS ref. no. 01-070-0278). By annealing the particles at 300°C, the diffraction peaks became more intense and sharper due to increase in crystallinity of $Y(OH)CO_3$ phase (Fig. S6a). In the literature it has been reported that by conventional homogenous urea precipitation method the phase of the as prepared particles is expected to be $Y(OH)CO_3$ or $Y(OH)CO_3.nH_2O$ only in amorphous phase due to the low degree of crystallinity of precursors synthesized by conventional precipitation method as compared to microwave assisted precipitation method [16,33,38,39]. In the XRD pattern of the particles calcined at 500°C, four weak and broad peaks at 2θ = 29.1, 33.7, 48.5, and 57.6 ° are present. The peaks can be assigned to (222), (400), (440), and (622) reflections of cubic Y_2O_3 which is an indication that $Y(OH)CO_3$ has decomposed into Y_2O_3 although with a low crystallinity. For the samples calcined at 600°C, all the diffraction peaks can be indexed as pure body-centred cubic (bcc) phase of Y_2O_3 [space group: *Ia*3(206)] (JCPDS: 01-073-1334). Increasing the calcination temperature to 900°C the intensity of the diffraction peaks increased and the width

narrowed (Fig. S6b), which indicates that the crystallinity and the crystallite size increases with increasing calcination temperature. These results are in agreement with the FTIR spectra which showed a phase transformation starting at 500°C and completed at 800°C.

The crystallite size was calculated using Scherrer equation [40] from the strongest peak (222) at (2θ=29.23°). The average crystallite size for samples calcined at different temperatures are summarized in Table 2, which shows an increasing crystallite size from ~8 nm to ~37 nm as the calcination temperature increased from 500°C to 900°C.

3.2.4. Transmission Electron Microscopy (TEM)

In order to confirm the FTIR and XRD data we further analysed by TEM the particles calcined at 700°C to 900°C for 2 hours (Fig. 7). The diameter of the $Y(OH)CO_3$ particles decreased by ~ 23±3% after calcination probably due to the phase transformation in Y_2O_3 particles (with higher density). The decrease in size from precursor to relevant oxide through thermal decomposition is well-reported in the literature [15,16,35]. However, the morphology of the particles did not change significantly by thermal treatment the spherical shape being maintained. Even particles calcined at 900°C are well dispersed with no aggregation observed probably due to the fact that higher activation energy is needed for the collapse of spherical morphology of the particles [40]. Higher magnification TEM analysis (insert Fig. 7c) confirmed that the particles are polycrystalline, consisting of smaller crystallites of ~40 nm for particles calcined at 900°C, which is in good agreement with crystallite size calculated from the XRD patterns.

3.3. $Y_2O_3:Eu^{3+}$ doped particles

Using the parameters obtained from the optimization of the microwave synthesis method $Y_2O_3:Eu^{3+}$ particles were produced by replacing 5% (molar percentage) of yttrium nitrate by europium nitrate. XRD pattern of $Y_2O_3:Eu^{3+}$ after calcination at 900°C for 2 hours (Fig. S6c) showed cubic Y_2O_3 phase with no detectable impurity phases. $Y_2O_3:Eu^{3+}$ particles with different sizes were synthesized by changing the ***u***. A similar polycrystalline structure and morphology similar to that of Y_2O_3 is observed (Fig. 8 and insert of Fig. 8). Furthermore, luminescent properties of $Y_2O_3:Eu^{3+}$ particles calcined at 900°C were investigated. The UV-Vis absorption spectrum shows a broad and prominent absorption band with a maximum absorption at ~235 nm (Fig. 9a). The absorption band is attributed to the transition between

the valence band and the conduction band [6]. Using UV-Vis absorption maximum the emission spectra of Y_2O_3:Eu^{3+} particles under UV excitation of 235 nm was measured at room temperature (Fig. 9b). Y_2O_3:Eu^{3+} particles exhibit a strong red emission centered at 613 nm the spectra showing characteristic optical properties of Eu^{3+} ions in the cubic Y_2O_3 host structure [41]. The emission spectrum is composed of $^5D_0 \rightarrow {}^7F_J$ (J=0, 1, 2, 3, 4) transition lines of Eu^{3+} ions, the strongest peak at 613 nm being attributed to the forced electronic dipole transition of $^5D_0 \rightarrow {}^7F_2$ predicted by Judd-Ofelt selection rules [14,15,38,42,43].

4. Conclusions

Microwave assisted urea precipitation method was used to obtain monodispersed $Y(OH)CO_3$ particles with spherical morphology. By optimizing the reaction parameters as: metal ions concentration, urea/metal ions ratio, temperature and reaction time we precisely controlled the size, shape and size distribution of the obtained nanospheres. The as prepared $Y(OH)CO_3$ particle decomposed to the cubic Y_2O_3 after heat treatment at the temperatures above 600°C preserving their shape and size monodispersity. Furthermore, using the optimized parameters for the synthesis of Y_2O_3 particles we synthesized Y_2O_3:Eu^{3+} nanocrystalline spheres of 100 nm to 350 nm diameter. The photoluminescence analysis of the doped nanocrystalline spheres showed that the Y_2O_3:Eu^{3+} particles have a strong red emission peak of Eu^{3+} ions at 613nm, due to the $^5D_0 \rightarrow {}^7F_2$ electronic dipole transition of Eu^{3+} ions. Moreover, due to their spherical shape, narrow particle size distribution and non agglomeration they can potentially be used for bioimaging and in display devices.

The microwave assisted urea precipitation technique used in this paper is a green, energy efficient and high reproducibility synthesis method. The optimized parameters can be used to produce any rare earth doped Y_2O_3 particles with tailored morphology, size and luminescent properties.

References:

[1] S. Zhong, J. Chen, S. Wang, Q. Liu, Y. Wang, S. Wang, Y_2O_3:Eu^{3+} hexagonal microprisms: Fast microwave synthesis and photoluminescence properties, J. Alloys Compd. 493 (2010) 322–325. doi:10.1016/j.jallcom.2009.12.092.

[2] P.F.S. Pereira, M.G. Matos, L.R. Ávila, E.C.O. Nassor, A. Cestari, K.J. Ciuffi, et al., Red, green and blue (RGB) emission doped $Y_3Al_5O_{12}$ (YAG) phosphors prepared by

non-hydrolytic sol–gel route, J. Lumin. 130 (2010) 488–493. doi:10.1016/j.jlumin.2009.10.019.

[3] V. Kumar Rai, A. Pandey, R. Dey, Photoluminescence study of Y_2O_3:Er^{3+}-Eu^{3+}-Yb^{3+} phosphor for lighting and sensing applications, J. Appl. Phys. 113 (2013) 083104. doi:10.1063/1.4793265.

[4] S. Som, S.K. Sharma, T. Shripathi, Influences of doping and annealing on the structural and photoluminescence properties of Y_2O_3 nanophosphors., J. Fluoresc. 23 (2013) 439–50. doi:10.1007/s10895-013-1160-7.

[5] T.S. Atabaev, Y.-H. Hwang, H.-K. Kim, Color-tunable properties of Eu^{3+}- and Dy^{3+}-codoped Y_2O_3 phosphor particles., Nanoscale Res. Lett. 7 (2012) 556. doi:10.1186/1556-276X-7-556.

[6] R.H. Krishna, B.M. Nagabhushana, H. Nagabhushana, N.S. Murthy, S.C. Sharma, C. Shivakumara, et al., Effect of Calcination Temperature on Structural, Photoluminescence, and Thermoluminescence Properties of Y_2O_3:Eu^{3+} Nanophosphor, J. Phys. Chem. C. 117 (2013) 1915–1924. doi:10.1021/jp309684b.

[7] A. Pandey, V.K. Rai, Improved luminescence and temperature sensing performance of Ho^{3+}-Yb^{3+}-Zn^{2+}: Y_2O_3 phosphor., Dalton Trans. 42 (2013) 11005–11. doi:10.1039/c3dt50592h.

[8] L. Robindro Singh, R.S. Ningthoujam, V. Sudarsan, I. Srivastava, S. Dorendrajit Singh, G.K. Dey, et al., Luminescence study on Eu^{3+} doped Y_2O_3 nanoparticles: particle size, concentration and core-shell formation effects., Nanotechnology. 19 (2008) 055201. doi:10.1088/0957-4484/19/05/055201.

[9] R. Li, L. Li, J. Wang, Z. Li, Q. Liu, J. Yu, et al., Influence of morphology and Yb^{3+} concentration on blue and red luminescence of uniform cube-like Y_2O_3:Yb^{3+}/Tm^{3+} particles, Mater. Chem. Phys. 141 (2013) 990–996. doi:10.1016/j.matchemphys.2013.06.043.

[10] C.A. Kodaira, A.V.S. Lourenço, M.C.F.C. Felinto, E.M.R. Sanchez, F.J.O. Rios, L.A.O. Nunes, et al., Biolabeling with nanoparticles based on Y_2O_3: Nd^{3+} and luminescence detection in the near-infrared, J. Lumin. 131 (2011) 727–731. doi:10.1016/j.jlumin.2010.11.026.

[11] S. Mukherjee, V. Sudarsan, R.K. Vatsa, S. V Godbole, R.M. Kadam, U.M. Bhatta, et al., Effect of structure, particle size and relative concentration of Eu^{3+} and Tb^{3+} ions on the luminescence properties of Eu^{3+} co-doped Y_2O_3:Tb nanoparticles., Nanotechnology. 19 (2008) 325704. doi:10.1088/0957-4484/19/32/325704.

[12] N. Venkatachalam, T. Yamano, E. Hemmer, H. Hyodo, H. Kishimoto, K. Soga, Er^{3+} -Doped Y_2O_3 Nanophosphors for Near-Infrared Fluorescence Bioimaging Applications, J. Am. Ceram. Soc. 96 (2013) 2759–2765. doi:10.1111/jace.12476.

[13] T.-L. Phan, M.-H. Phan, N. Vu, T.-K. Anh, S.-C. Yu, Luminescent properties of Eu-doped Y_2O_3 nanophosphors, Phys. Status Solidi. 201 (2004) 2170–2174. doi:10.1002/pssa.200406825.

[14] H. Yoo, H. Jang, W. Im, Particle size control of a monodisperse spherical Y_2O_3: Eu^{3+} phosphor and its photoluminescence properties, J. Mater. Res. 22 (2007) 2017–2024. doi:10.1557/JMR.2007.0257.

[15] J. Yang, Z. Quan, D. Kong, X. Liu, J. Lin, Y_2O_3□: Eu^{3+} Microspheres: Solvothermal Synthesis and Luminescence Properties, Cryst. Growth Des. 7 (2007) 730–735. doi:10.1021/cg060717j.

[16] T. Yan, D. Zhang, L. Shi, H. Yang, H. Mai, J. Fang, Reflux synthesis, formation mechanism, and photoluminescence performance of monodisperse Y_2O_3:Eu^{3+} nanospheres, Mater. Chem. Phys. 117 (2009) 234–243. doi:10.1016/j.matchemphys.2009.05.047.

[17] X. Hou, S. Zhou, Y. Li, W. Li, Luminescent properties of nano-sized Y_2O_3:Eu fabricated by co-precipitation method, J. Alloys Compd. 494 (2010) 382–385. doi:10.1016/j.jallcom.2010.01.054.

[18] J. Zhang, Z. Zhang, Z. Tang, Y. Lin, Z. Zheng, Luminescent properties of Y_2O_3:Eu synthesized by sol–gel processing, J. Mater. Process. Technol. 121 (2002) 265–268. doi:10.1016/S0924-0136(01)01263-8.

[19] N. Vu, T. Kim Anh, G.-C. Yi, W. Strek, Photoluminescence and cathodoluminescence properties of Y_2O_3:Eu nanophosphors prepared by combustion synthesis, J. Lumin. 122-123 (2007) 776–779. doi:10.1016/j.jlumin.2006.01.286.

[20] L. Wang, L. Shi, N. Liao, H. Jia, P. Du, Z. Xi, et al., Photoluminescence properties of Y_2O_3:Tb^{3+} and YBO_3:Tb^{3+} green phosphors synthesized by hydrothermal method, Mater. Chem. Phys. 119 (2010) 490–494. doi:10.1016/j.matchemphys.2009.10.002.

[21] D. Dosev, B. Guo, I.M. Kennedy, Photoluminescence of as an indication of crystal structure and particle size in nanoparticles synthesized by flame spray pyrolysis, J. Aerosol Sci. 37 (2006) 402–412. doi:10.1016/j.jaerosci.2005.08.009.

[22] T. Hirai, Y. Asada, I. Komasawa, Preparation of Y_2O_3:Eu^{3+} nanoparticles in reverse micellar systems and their photoluminescence properties., J. Colloid Interface Sci. 276 (2004) 339–45. doi:10.1016/j.jcis.2004.03.070.

[23] M. Raukas, a. Konrad, K.C. Mishra, Luminescence in nano-size Y_2O_3:Ce, J. Lumin. 122-123 (2007) 773–775. doi:10.1016/j.jlumin.2006.01.285.

[24] F.-W. Liu, C.-H. Hsu, F.-S. Chen, C.-H. Lu, Microwave-assisted solvothermal preparation and photoluminescence properties of Y_2O_3:Eu^{3+} phosphors, Ceram. Int. 38 (2012) 1577–1584. doi:10.1016/j.ceramint.2011.09.044.

[25] M. Serantoni, E. Mercadelli, A.L. Costa, M. Blosi, L. Esposito, A. Sanson, Microwave-assisted polyol synthesis of sub-micrometer Y_2O_3 and Yb- Y_2O_3 particles for laser

source application, Ceram. Int. 36 (2010) 103–106. doi:10.1016/j.ceramint.2009.07.002.

[26] A. Vadivel Murugan, A.K. Viswanath, V. Ravi, B.A. Kakade, V. Saaminathan, Photoluminescence studies of Eu^{3+} doped Y_2O_3 nanophosphor prepared by microwave hydrothermal method, Appl. Phys. Lett. 89 (2006) 123120. doi:10.1063/1.2356694.

[27] M. Rekha, K. Laishram, R.K. Gupta, N. Malhan, A.K. Satsangi, Energy-efficient green synthesis of Nd: Y_2O_3 nanopowder by microwave gel combustion, J. Mater. Sci. 44 (2009) 4252–4257. doi:10.1007/s10853-009-3615-4.

[28] Y.-P. Fu, Ionic conductivity and mechanical properties of Y_2O_3-doped CeO_2 ceramics synthesis by microwave-induced combustion, Ceram. Int. 35 (2009) 653–659. doi:10.1016/j.ceramint.2008.01.027.

[29] L. Ma, W. Chen, J. Zhao, Y. Zheng, X. Li, Z. Xu, Microwave-assisted synthesis of praseodymium hydroxide nanorods and thermal conversion to oxide nanorod, Mater. Lett. 61 (2007) 1711–1714. doi:10.1016/j.matlet.2006.07.116.

[30] B.L. Cushing, V.L. Kolesnichenko, C.J. O'Connor, Recent advances in the liquid-phase syntheses of inorganic nanoparticles., Chem. Rev. 104 (2004) 3893–946. doi:10.1021/cr030027b.

[31] A.S. Vanetsev, E.P. Butkina, A.E. Baranchikov, A.S. Shaporev, A. V. Dzuban, M.A. Soldatov, et al., Microwave-assisted synthesis of spherically shaped monodisperse Y_2O_3 and Y_2O_3:Eu powders, Dokl. Chem. 424 (2009) 35–38. doi:10.1134/S0012500809020049.

[32] A.L. Costa, M. Serantoni, M. Blosi, E. Mercadelli, L. Esposito, A. Piancastelli, et al., Microwave Assisted Synthesis of Yb: Y_2O_3 Based Materials for Laser Source Application, Adv. Eng. Mater. 12 (2010) 205–209. doi:10.1002/adem.200900272.

[33] D. Sordelet, M. Akinc, Preparation of Spherical , Monosized Y_2O_3 Precursor Particles, J. Colloid Interface Sci. 122 (1988) 47–59.

[34] X. Jing, T. Ireland, C. Gibbons, Control of Y_2O_3: Eu spherical particle phosphor size, assembly properties, and performance for FED and HDTV, J. Electochemical Soc. 146 (1999) 4654–4658. http://jes.ecsdl.org/content/146/12/4654.short (accessed August 06, 2014).

[35] M. Xing, W. Cao, H. Zhong, Y. Zhang, X. Luo, Y. Fu, et al., Synthesis and upconversion luminescence properties of monodisperse Y_2O_3:Yb, Ho spherical particles, J. Alloys Compd. 509 (2011) 5725–5730. doi:10.1016/j.jallcom.2011.02.135.

[36] D. Zhao, Q. Yang, Z. Han, F. Sun, K. Tang, F. Yu, Rare earth hydroxycarbonate materials with hierarchical structures: Preparation and characterization, and catalytic activity of derived oxides, Solid State Sci. 10 (2008) 1028–1036. doi:10.1016/j.solidstatesciences.2007.11.019.

[37] Y. Zhang, M. Gao, K. Han, Z. Fang, X. Yin, Z. Xu, Synthesis, characterization and formation mechanism of dumbbell-like $YOHCO_3$ and rod-like $Y_{2(}CO_3)_3 \cdot 2.5H2O$, J. Alloys Compd. 474 (2009) 598–604. doi:10.1016/j.jallcom.2008.07.007.

[38] G. Jia, H. You, Y. Song, Y. Huang, M. Yang, H. Zhang, Facile synthesis and luminescence of uniform Y_2O_3 hollow spheres by a sacrificial template route., Inorg. Chem. 49 (2010) 7721–5. doi:10.1021/ic100430g.

[39] L.S. Chi, R.S. Liu, B.J. Lee, Synthesis of Y_2O_3:Eu, Bi Red Phosphors by Homogeneous Coprecipitation and Their Photoluminescence Behaviors, J. Electrochem. Soc. 152 (2005) J93. doi:10.1149/1.1940752.

[40] J. Zhang, S. Wang, Upconversion luminescence in Er^{3+} doped and Yb^{3+}/Er^{3+} codoped yttria nanocrystalline powders, J. Am. Ceram. Soc. 1075 (2004) 1072–1075. http://onlinelibrary.wiley.com/doi/10.1111/j.1551-2916.2004.01072.x/abstract (accessed August 06, 2014).

[41] J. Chen, F. Gu, W. Shao, C. Li, Hydrothermal synthesis of ordered nanolamella-composed Y_2O_3:Eu^{3+} architectures and their luminescent properties, Phys. E Low-Dimensional Syst. Nanostructures. 41 (2008) 304–308. doi:10.1016/j.physe.2008.07.020.

[42] M.L. Pang, J. Lin, Z.Y. Cheng, J. Fu, R.B. Xing, S.B. Wang, Patterning and luminescent properties of nanocrystalline Y_2O_3:Eu^{3+} phosphor films by sol–gel soft lithography, Mater. Sci. Eng. B. 100 (2003) 124–131. doi:10.1016/S0921-5107(03)00081-3.

[43] A. Boukerika, L. Guerbous, Annealing effects on structural and luminescence properties of red Eu^{3+}-doped Y_2O_3 nanophosphors prepared by sol–gel method, J. Lumin. 145 (2014) 148–153. doi:10.1016/j.jlumin.2013.07.037.

Table captions:

Table 1. Effect of [urea]/[Y3+], u, and reaction temperature on the particle size.

Table 2. The FWHM of (222) peak and crystallite size from XRD patterns shown in Fig. 6.

Figure captions:

Fig. 1. TEM micrographs of as prepared particles with $[Y^{3+}]$=0.005 M and reaction time of 15 minutes for different ***u*** and reaction temperature of: a) ***u***=10, 80°C, b) ***u***=20, 80°C, c) ***u***=20, 90°C, d) ***u***=50, 90°C, e) ***u***=60, 90°C, f) ***u***=80, 100°C, (The length of the scale bar represents 200 nm).

Fig. 2. The relationship between ***u***, reaction temperature and particle size for a fixed $[Y^{3+}]$ concentration of a) 0.005 M, b) 0.02 M.

Fig. 3. The relationship between a) [Y^{3+}] concentration and particle size for a fixed urea concentration (0.04 M), 90°C reaction temperature and 15 minutes reaction time, and b) reaction time and particle size for a fixed ***u***=40, [Y^{3+}]=0.01 M and 90°C reaction temperature.

Fig. 4. TGA thermogram of as prepared particles with different ***u***.

Fig. 5. FTIR spectra of as prepared particles and calcined particles at different temperatures (from 300°C to 900°C for 2 hours).

Fig. 6. XRD patterns of as prepared particles and particles calcined at different temperatures (from 300°C to 900°C for 2 hours).

Fig. 7. TEM micrographs of Y_2O_3 particles calcined at 700°C, b) 800°C, c) 900°C for 2 hours, (The length of the scale bar represents 100 nm).

Fig. 8. TEM micrographs of Y_2O_3:Eu^{3+} particles calcined at 900°C synthesized with different ***u***, a) ***u***=50, size 98 ± 12 nm, b) ***u***=40, size 173 ± 18 nm, c) ***u***=30, size 232 ± 26 nm, (The length of the scale bar represents 200 nm).

Fig. 9. a) UV-Vis absorption and b) PL spectrum of Y_2O_3:Eu^{3+} particles calcined at 900°C for 2 hours.

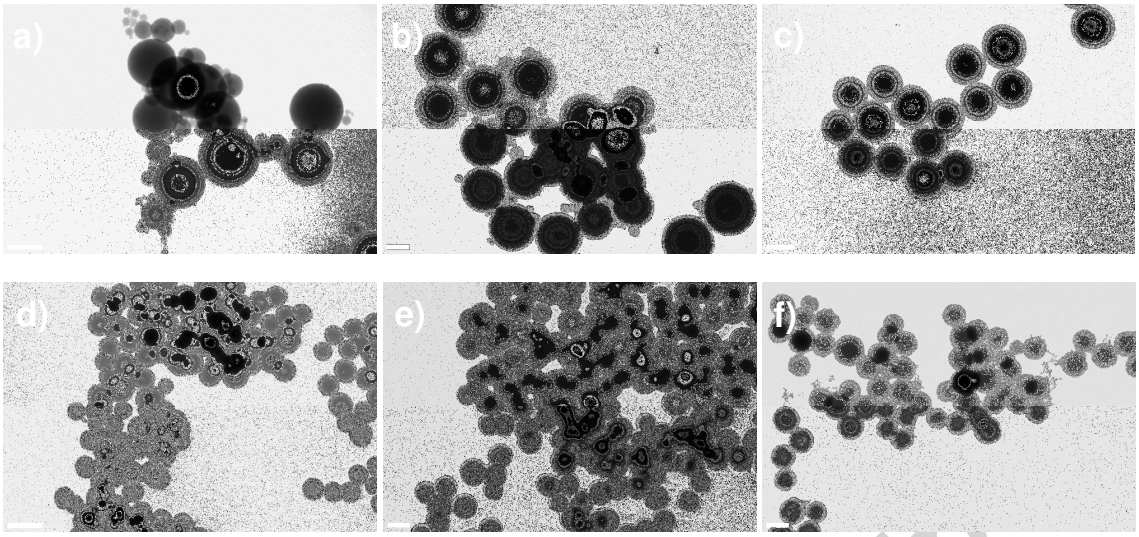

Fig. 1.

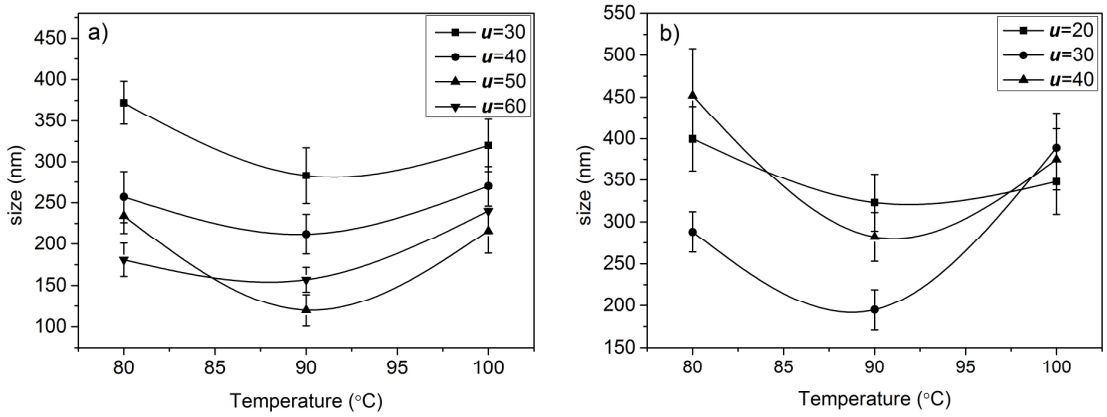

Fig. 2.

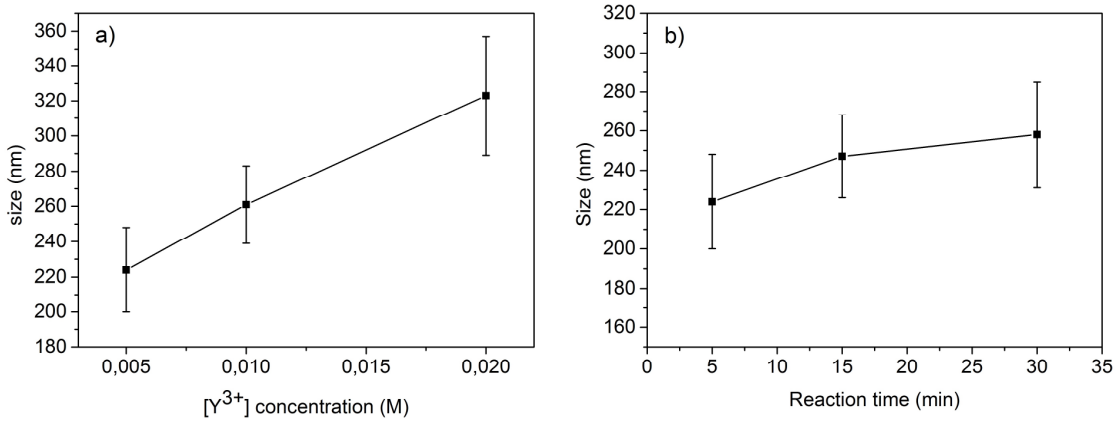

Fig. 3.

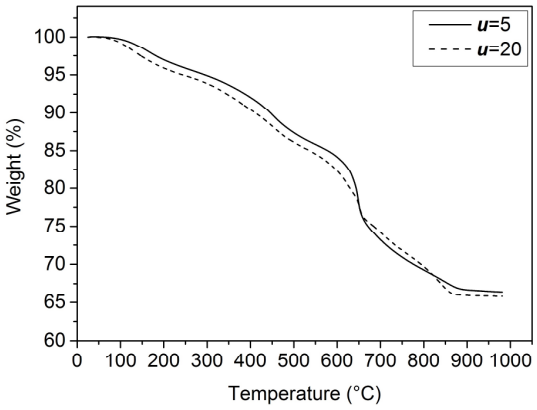

Fig. 4.

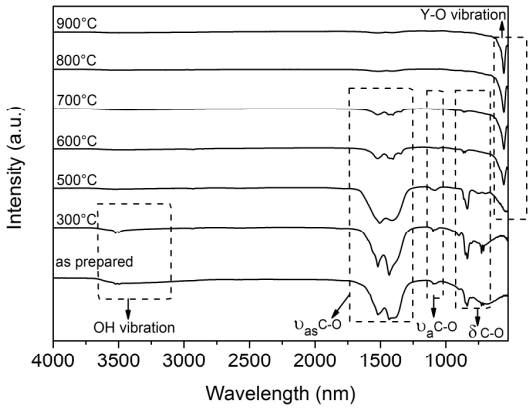

Fig. 5.

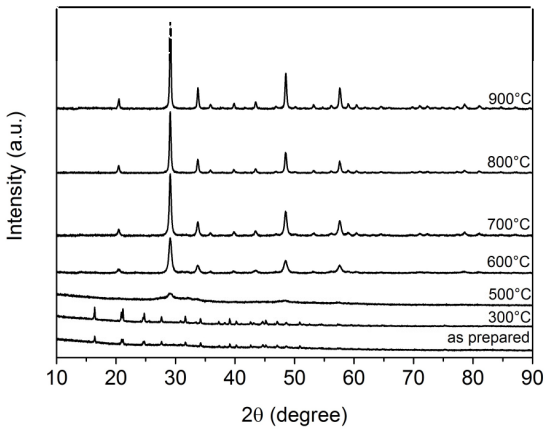

Fig. 6.

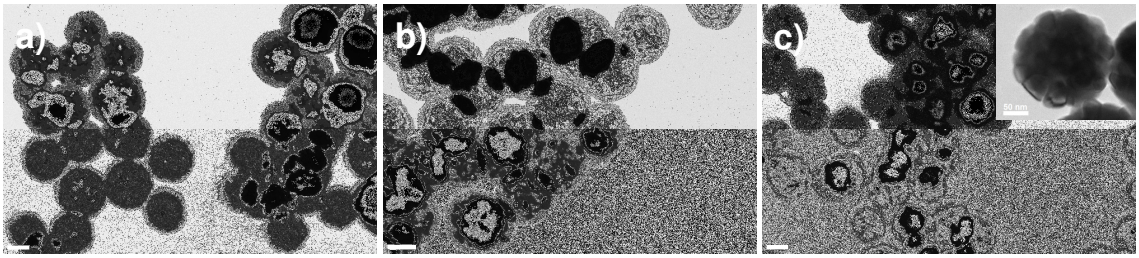

Fig. 7.

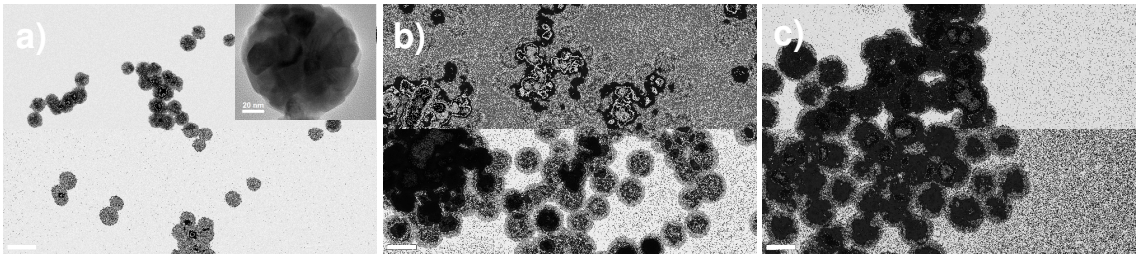

Fig. 8.

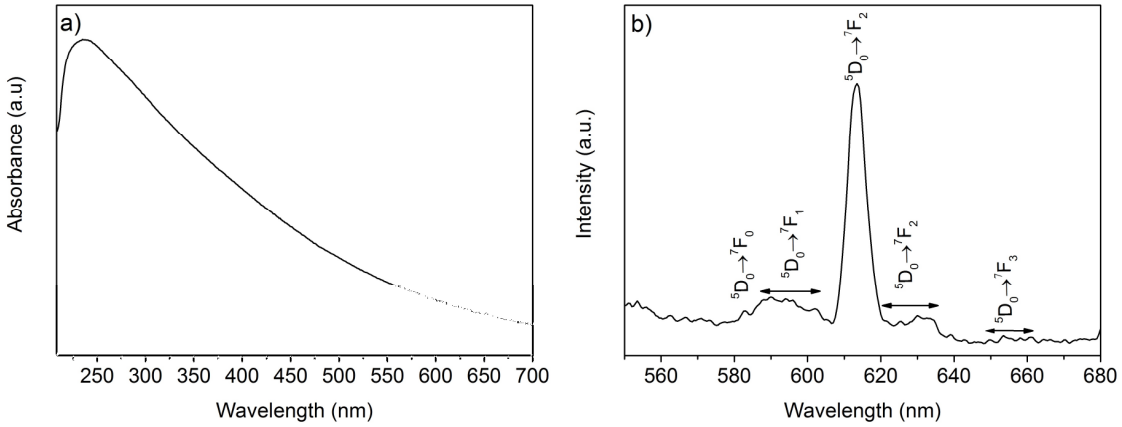

Fig. 9.

Table 1.

$[Y^{3+}]$ concentration [M]	$[urea]/[Y^{3+}]$ molar ratio, ***u***	Particle size (nm)		
		Reaction temp. (80°C)	Reaction temp. (90°C)	Reaction temp. (100°C)
0.02	20	400 ± 39	323 ± 34	348 ± 39
0.02	30	288 ± 24	195 ± 24	389 ± 42
0.02	40	452 ± 56	282 ± 29	375 ± 37
0.005	30	372 ± 26	283 ± 34	320 ± 32
0.005	40	257 ± 31	212 ± 24	270 ± 24
0.005	50	234 ± 21	120 ± 19	216 ± 27
0.005	60	181 ± 20	157 ± 15	240 ± 27

Table 2.

Calcination temperature (°C)	500	600	700	800	900
FWHM of (222) peak (2θ)	1.05	0.47	0.31	0.26	0.22
Crystallite size (nm)	7.8	17.4	26.4	31.8	36.8